Nano Materials Science 6 (2024) 24–37

Contents lists available at ScienceDirect

Nano Materials Science

journal homepage: www.keaipublishing.com/cn/journals/nano-materials-science/

Aerosol deposition technology and its applications in batteries

Xinyu Wang [a,b], Ramon Alberto Paredes Camacho [a], Xiaoyu Xu [a,b], Yumei Wang [a], Yi Qiang [a], Hans Kungl [c], Ruediger-A. Eichel [c], Yunfeng Zhang [a,b,*], Li Lu [a,b,**]

[a] National University of Singapore (Chongqing) Research Institute, Chongqing, 401123, PR China
[b] National University of Singapore, Singapore, 117576
[c] Fundamental Electrochemistry (IEK-9), Institute of Energy and Climate Research, Forschungszentrum Jülich, 52425, Jülich, Germany

ARTICLE INFO

Keywords:
Aerosol deposition
Room temperature impact consolidation
Ceramic film
All-solid-state battery
Spray coating technology

ABSTRACT

Aerosol deposition (AD) method is a kind of additive manufacturing technology for fabricating dense films such as metals and ceramics at room temperature. It resolves the challenge of integrating ceramic films onto temperature-sensitive substrates, including metals, glasses, and polymers. It should be emphasized that the AD is a spray coating technology that uses powder without thermal assistance to generate films with high density. Compared to the traditional sputter-based approach, the AD shows several advantages in efficiency, convenience, better interfacial bonding and so on. Therefore, it opens some possibilities to the field of batteries, especially all-solid-state batteries (ASSBs) and draws much attention not only for research but also for large scale applications.

The purpose of this work is to provide a critical review on the science and technology of AD as well as its applications in the field of batteries. The process, mechanism and effective parameters of AD, and recent developments in AD applications in the field of batteries will be systematically reviewed so that a trend for AD will be finally provided.

1. Introduction

In general, it is difficult to produce monolithic ceramic structures integrated with low melting point materials such as metals, glasses and polymers using conventional methods because ceramic materials typically require thermal assistance above 1000 °C [1]. Additionally, traditional thick ceramic films frequently suffer from mechanical reliability and failures due to poor adhesion, leading to easily peel off from substrates. Therefore, the interfacial bounding between ceramic films and other components or substrates is particularly important. These issues can be addressed using a technique known as Aerosol deposition (AD) that is also sometimes referred to as vacuum cold spraying (VCS), vacuum kinetic spraying (VKS) or powder aerosol deposition (PAD) [2,3]. AD is a kind of additive manufacturing method, namely spraying coating method at room temperature. To achieve a desirable adhesion, the solid-state particles are accelerated to a super-sonic velocity by carrier gas in a low vacuum condition. Then particles have ballistic impingement onto substrate to form a film. A dense ceramic film could be created at room temperature from raw powder without any thermal assistance in this process. These films preserve practically all the characteristics of the initial materials, making this method suitable for a wide range of uses [4].

Primordially, a deposition method of ultra-fine particles using a gas jet was proposed in 1984 by Seiichiro Kashu et al. Ultra-fine metal or ceramic particles of diameter of less than 1 μm were utilized to deposit on a solid surface. This serves as an illustrative example of how this method can result in the creation of a film with an increased dielectric constant [5]. The first application related to jet-printed was published in 1997 [6]. For the purpose of actuating micro-electromechanical systems (MEMS), lead zirconate titanate (PZT) films were fabricated on metal or ceramic substrate using this method, demonstrating superior ferroelectric and piezoelectric properties [7]. The X-ray diffraction (XRD) and scan electron microscopy (SEM) revealed that the perovskite structure of the PZT remained the same before and after deposition [8]. Only in 1999, the terminology of “Aerosol Deposition” was put forward by Akedo and his group [3]. Later they continued to investigate the principle of AD and densification mechanism of ceramic films. The principle of “room temperature impact consolidation” (RTIC) was proposed [9]. Since its initial development, this technology has undergone significant advances in both of process and applications with continuous innovation and expansion by

* Corresponding author. National University of Singapore (Chongqing) Research Institute, Chongqing, 401123, PR China.
** Corresponding author. National University of Singapore (Chongqing) Research Institute, Chongqing, 401123, PR China.
E-mail addresses: mpezyf@nus.edu.sg (Y. Zhang), luli@nus.edu.sg (L. Lu).

https://doi.org/10.1016/j.nanoms.2023.11.002
Received 21 August 2023; Accepted 9 November 2023
Available online 29 November 2023

researchers worldwide. Today, AD applications can be used across various fields, including electronics, energy devices, biomedical engineering, and numerous other sectors in both research and industries [10,11]. Although several reviews on AD technology have been published, there is still lack of understanding of fundamentals and mechanisms, and applications of AD, particularly in the area of energy storage. Therefore, this work focuses on the above three important concerns.

Fig. 1 summarizes the merits of AD over conventional ceramic film production methods. Firstly, it is a deposition process operated at room temperature, allowing to produce films on a wide range of substrates without risking damage from high temperatures. Any substrate can be practically and simply used to manufacture ceramic films by AD. Secondly, it can achieve good adhesion without diffusion interface. The adhesion between the aerosol-deposited (ADed) film and substrate is strong and it is able to surmount a bunch of hurdles in interface reducing the risk of chemical reactions and ensuring long-term stability. Thirdly, the ADed films have a highly dense and nanocrystalline structure, which enhances their mechanical, electrical, and thermal properties. Finally, due to room temperature deposition, it demonstrates high efficiency and conveniency. The whole process can be carried out at room temperature in a much short period of deposition.

For the purpose of coating ceramic films, a variety of deposition methods are available, such as plasma spraying (PS) [12], pulsed laser deposition (PLD) [13,14], ion-beam deposition [15,16], chemical vapor deposition (CVD) [17], cold spray (CS) [18,19] and so on. Table 1 summarizes the features for different deposition methods for ceramic film production.

Some kinds of spraying methods are assumed to be the mature technologies whose essential processes and mechanisms have been observed and described adequately. PS and CVD equipment are already being produced commercially. A wide range of their products have been used in various commercial applications. CS is the most similar spraying method as the AD, which also uses particles with high velocity and small size to form bonding [20,21]. Compared with other spraying methods, the AD has advantages in simple operating process and low temperature requirement. Although the film growth rate using the AD is high, the efficiency of utilization of powder during AD is still low at present since a portion of powder is unable to be deposited onto the film but flies away to deposition chamber. How to recycle the powder is the key issue to improve the deposition efficiency. It is still in a developing stage with uncertainty both in process and mechanism, which attracts numerous researchers to explore further.

Recently AD technology has been further studied for the processing for the energy storage devices to challenge shortage and pollution of fossil fuels [22]. The current rechargeable batterie are known to have safety issue, low capacity and short life-cycle problems due mainly to a number of factors including flammable organic electrolyte and use of nonconductive polymer binder [23,24]. Owing to the unique characters, AD provides more options in the fabrication of better batteries. The applications of AD in electrode, electrolyte, and hence all-solid-state batteries (ASSBs) are shown in Fig. 2. Fig. 2(a) shows the morphology of

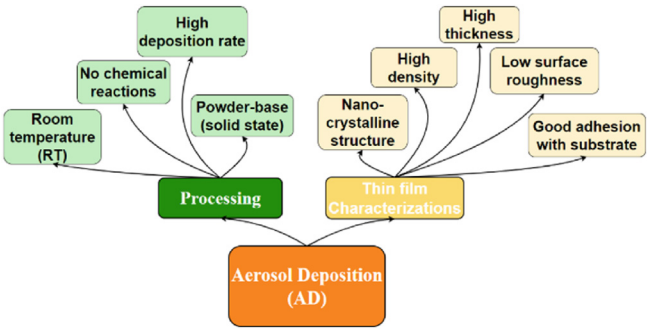

Fig. 1. Characteristics of aerosol deposition method.

aerosol-deposited (ADed) composite film electrode for lithium battery [25]. In contrast to the conventional techniques in battery processing, where polymeric binders are used in fabrication of the electrode layers, AD provides.

binder-free ceramic layer. Fig. 2(b) demonstrates deposition of the ceramic-based electrolyte $Li_{1.5}Al_{0.5}Ge_{1.5}(PO_4)_3$ (LAGP) on a stainless steel substrate with a low thickness via AD [26]. The ASSB prepared by AD is shown in Fig. 2(c). Electrode film of $LiCoO_2$ (LCO) is directly deposited on the solid-state electrolytes, $Li_7La_3Zr_2O_{12}$ (LLZO). This ASSB revealed good electrochemical performance in capacity (Fig. 2(d)) due to better contact between electrode and electrolyte [27].

2. AD apparatus and process

A schematic illustration showing a typical AD apparatus is displayed in Fig. 3, typically consisting of three primary parts: (1) an aerosol generation unit, which includes the aerosol generator and the gas supplier, in which the powder and gas are mixed to create aerosol, (2) a deposition chamber, which contains the nozzle and the mobile stage, where the powder particles from aerosol generator are accelerated and deposited on substrates, and (3) a vacuum system, which consists of a chamber and a pump in which the vacuum pump is utilized to create a low pressure in the deposition chamber whereas the carrier gas and deposition chamber are connected to the aerosol generating chamber. The delivery of aerosol with particles from the aerosol chamber to the deposition chamber is caused by the difference in pressures between the aerosol generator and deposition chamber. Each part's specifications and construction information will be discussed later.

The substrate is mounted in an X–Y moveable stage. The aerosol generating chamber is then filled with a carrier gas to create an aerosol that contains particles. The particles are accelerated by gas flow in aerosol generator at first. Then the particles and gas flow are accelerated again when they leave from the nozzle due to the pressure difference between the two chambers. The powder particles are then bombarded onto the substrate via a nozzle. Normally particles traveling with a supersonic speed between 200 and 600 m s^{-1} are propelled to substrates [4]. The room-temperature impact plays a significant role in consolidation to ensure particles adhesion to the substrates. A multilayer ADed film is produced by iteratively moving the substrate multiple times.

Although design and setup of an AD equipment are simple, AD process is complicated since it is not only associated with types of raw materials and substrates to be used but also to how the aerosol is generated and transported towards the substrate. Most of the AD devices have the similar basic mechanical construction, but some parts have different designs to produce films with targeted properties. Within all important considerations, the aerosol generating unit and the nozzle, are the major focus of the fabrication and enhancement of the AD machine.

To minimize porosity and increase homogeneity of ADed film, new designs of AD machine have also been investigated. A small-size and simplified device named as Micro-Powder Aerosol Deposition (μ-PAD) was produced [28]. This μ-PAD device uses flexible spot deposition by circular de Laval nozzle rather than moveable substrate components. It adapts a discontinuous operation mode, resulting in several seconds operation time to achieve a thicker film with much less powder quantity [29]. By this method, the surface profile is a Gaussian-shaped and the thickness can reach 1 μ m in one time single-shot deposition. Therefore, this μ-PAD method is better than conventional AD method for repairing damaged coatings with ceramic films at room temperature [30].

2.1. Aerosol generation unit

An important and crucial unit for the entire operation is the one that is able to generate uniform and continuous aerosol. This unit is intended to aerosolize powdered particles and to steadily deliver the homogenous aerosol to the deposition chamber. The particle size distribution and agglomeration play an important role on the deposition efficiency of film

Table 1
Features and parameters of different methods for ceramic film production.

methods	assisting devices	adhesion strength	materials	thickness of films	particle size	Temperature (C°)	pressure	deposition rate
Aerosol Deposition	no	Mechanical bonding	ceramic	1–200 μm	1–10 μm	RT	0.2–20 mbar	
Cold Spray	no	adiabatic shear instability	ceramic, metal, polymer	10–200 μm	200 nm		1 atm	
Plasma Spraying	plasma torch	solidification of the molten particles	ceramic, metal	200 μm-10mm	10–100 μm	5500–8300	1 atm	up to a few kg/h
Pulsed Laser Deposition (PLD)	pulsed-laser beam	solidification of the molten particles	ceramic, metal, polymer	200–400 nm		300–800	ultrahigh vacuum (UHV)/10^{-9} mbar	
Ion beam assisted Deposition (IBAD)	ion beam source		ceramic, metal, polymer	200 nm-20μm		800	10^{-7} mbar	0.05 $\mu m^3 s^{-1}$
Chemical Vapor Deposition	vapor generator	epitaxy, gas-phase precipitation	metal, carbides, nitrides, oxides	<1 μm	atoms or molecules	600–2000	0.2 mbar - 1 atm	high

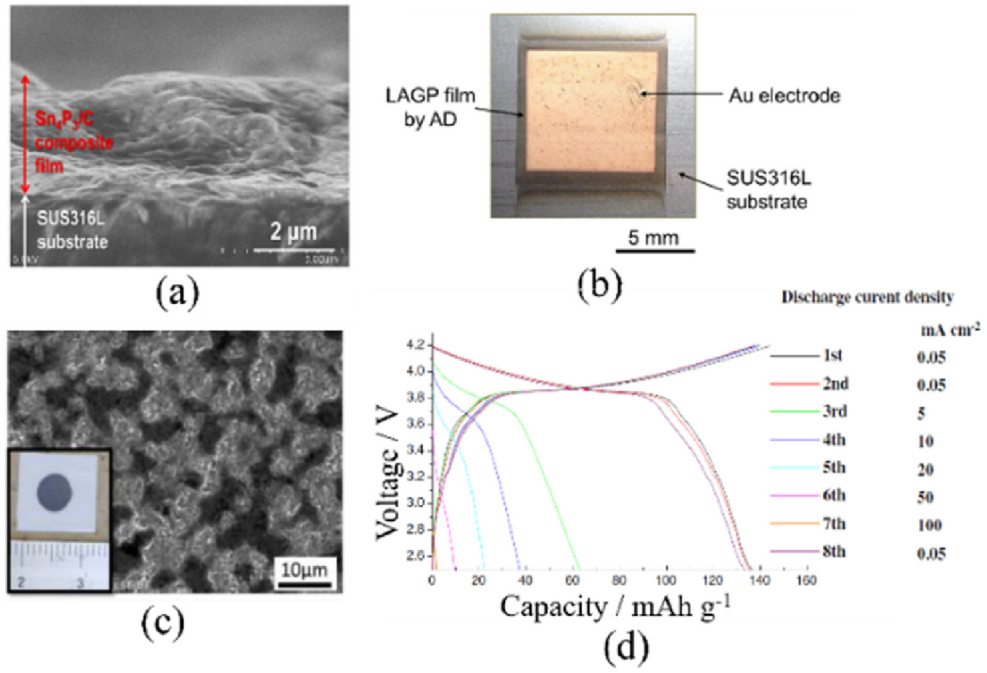

Fig. 2. Battery prepared by AD: (a) cross-sectional SEM image of Sn_4P_3/C composite electrode film [24], (b) Au electrode on ADed LAGP electrolyte [25], and (c) surface morphology of an ADed-LCO and (d) charge-discharge plots of all-solid-state battery (ADed LCO - LATP | LLZO | Li cell) [26].

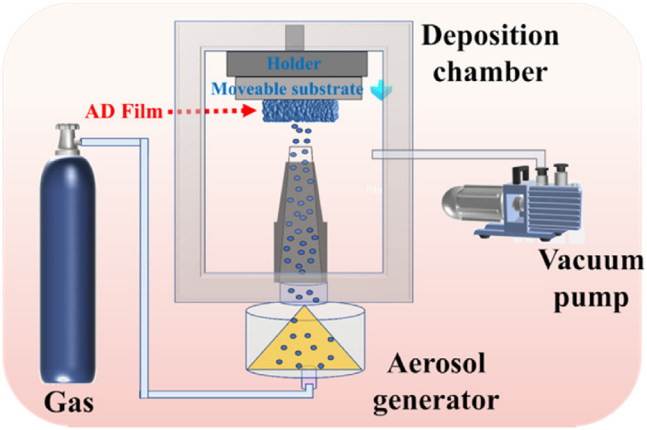

Fig. 3. Schematic illustration of the construction of an aerosol deposition system.

[31]. Owing to the small particle, typically ranging from 100 nm or slightly bigger, the particles tend to agglomerate in the reservoir, namely aerosol generating chamber, and flow tube. Agglomeration occurs as a result from the cohesive force between the particles due to van der Waals, electrostatic, capillary, viscous, adhesive, and so on [32]. To achieve monodispersed and continuous particles, it is critical to introduce external force, such as gas shear force, to prevent and destroy the agglomeration.

There are two kinds of typical aerosol generators using different principles to aerosolize particles, one of which is fluidized bed generator and another one is blush generator with powder dispersion unit as shown in Fig. 4 according to the comparison by Hanft et al. [33]. The fluidized bed generator is used in most cases due to the merits of simple structure and easy operation, but its aerosol concentration and feed rate cannot be controlled. Both of them decrease nonlinearly with operation time because the fine particles are extracted primarily but the large particles and agglomeration are extracted hardly. Some additional auxiliary methods are equipped on fluidized bed aerosol generator to alleviate this problem assisting in aerosolization, such as the vibrating table. The

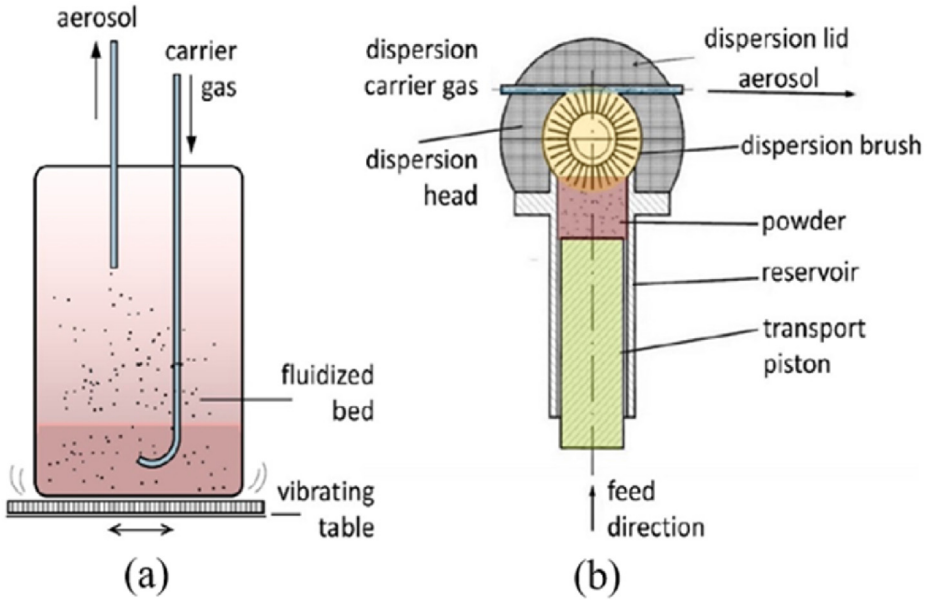

Fig. 4. Schematics of (a) fluidized bed aerosol generator and (b) blush generator [32].

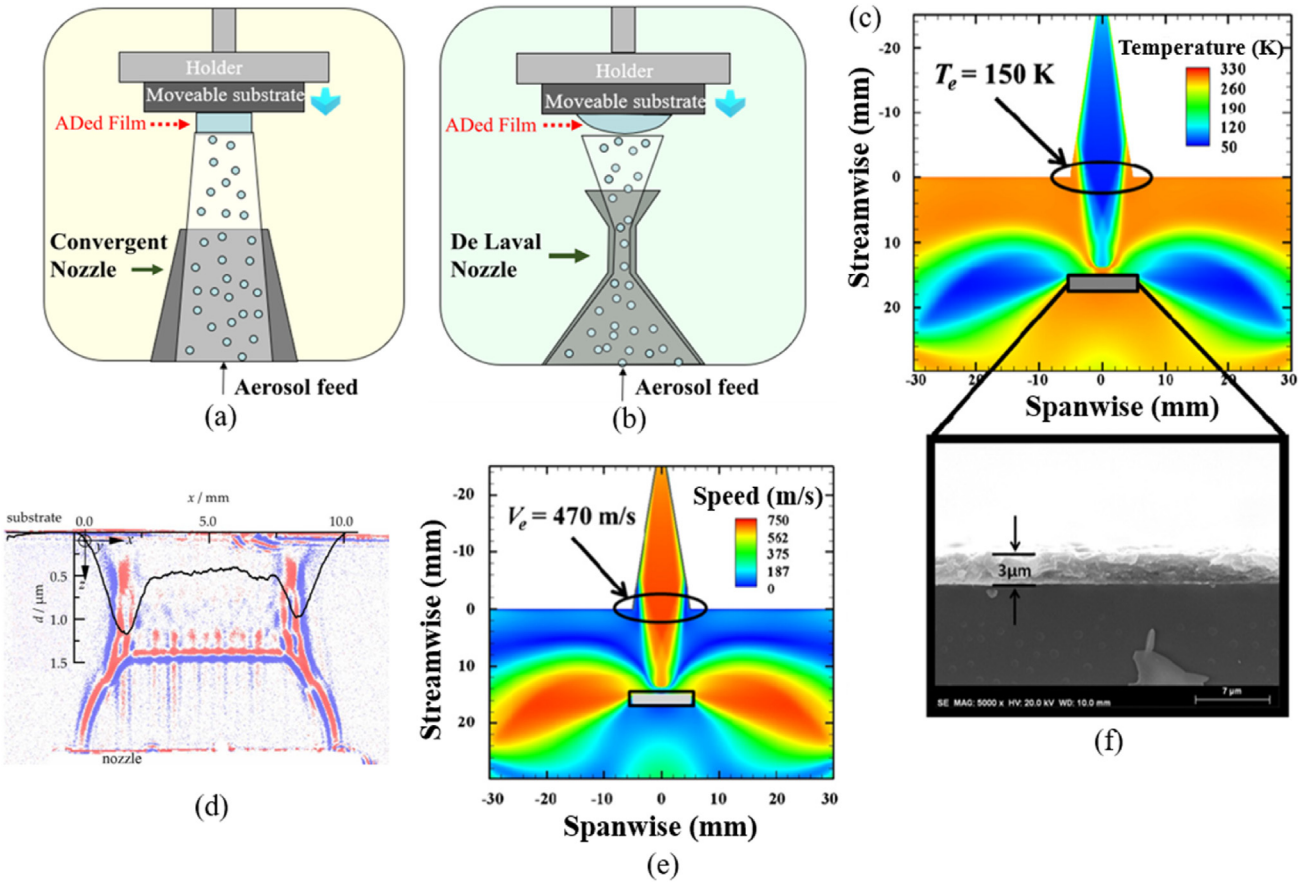

Fig. 5. Schematics of different types of Nozzles: (a) convergent nozzle and (b) de-Laval nozzle; CFD predictions: (c) gas speed, (e) temperature for the optimized nozzles and (f) their actual film of TiO_2 [34], (d) ADed film thickness profile (thickness (d) over width (x)) superposed with its corresponding expansion of carrier gas between the slit nozzle and stage by shadow image [36].

biggest advantage of the blush generator is better controllability and stability. The deposition rate is linearly related to prison velocity, aerosol concentration and time. However, the mechanical structure is too complex which may be more applicable for large scale production with a bigger powder reservoir. Hence, the fluidized bed aerosol generator is proper for AD in the research stage. The blush generator may play an important role in large-scale industrial production in the future.

2.2. Nozzle and stage

Another critical component is the nozzle that delivers the aerosol and accelerates the particles to final velocity on to the substrate. Since bonding between the particles and the substrate is closely related to the kinetic energy of the ejected powder based on the principle of room temperature impact consolidation (RTIC) [9], the velocity of the particles just before bombed on to the substrate determines the success of the deposition [34]. It has been noted that only the particles with appropriate velocities can be deposited on the substate successfully. If the velocity of particle is below the minimum critical velocity (V_{cr1}), the kinetic energy is insufficient to create adhesion strength between particles and substrate. Conversely, if the velocity of the particle exceeds maximum critical velocity (V_{cr2}), possible erosion may take place. Normally, their critical velocities in the range of V_{cr1}-V_{cr2} where V_{cr1} is 200 m s^{-1} and V_{cr2} is 600 m s^{-1}. Besides, these critical velocities also may change with properties of materials and substrates. The final velocities of particles are influenced and controlled by the geometry of the nozzle and stand-off distance from nozzle to stage during processing. Therefore, it is vitally important to optimize this component to achieve higher deposition efficiency.

Two types of nozzles, namely conventional convergent nozzle and de Laval convergent–divergent nozzle are commonly used in the AD. The schematic diagram and the two types of nozzles are shown in Fig. 5(a) and (b). As for convergent nozzle, the reachable velocity of gas is sound velocity by reason of chocking. On the other hand, the gas can be accelerated over the sound velocity after passing the throat in de Laval nozzle [34]. The de Laval nozzle for AD device can be optimized both experimentally and theoretically using computational fluid dynamics (CFD) [35]. The width and length of throat is the crucial part in design of de Laval nozzle. The pressure difference between the exit of a nozzle and deposition chamber will increase with width of throat decreases [36]. Only a "correctly-expanded" nozzle whose exit pressure is equal to ambient pressure will not generate the undesirable elements, such as shear layer, expansion fan and reflected compression shock, that reduce the deposition efficiency and quality of ADed films. Fig. 5(c) and (e) show the simulation results in pressure and temperature of optimally modified nozzle. The corresponding SEM image of titanium dioxide film fabricated by this kind of nozzle is shown in Fig. 5(f).

Furthermore, the stand-off distance between the nozzle and the stage needs to be optimized as well. When the substrate is too close to the nozzle exit, the shockwave generated by the aerosol flow can be reflected back by substrate and interfere with the subsequent gas flow and particles, leading to a decrease in deposition efficiency. The experimental results from shadow imaging method in Fig. 5(d) also indicated this view [37]. The shock generated in the gas flow are influenced by nozzle geometry and stand-off distance resulting uniformity of the ADed film.

All in all, Optimization of the nozzle geometry is critical in design of AD device to improve device performance and achieve deposition of films with targeted properties.

3. Processing parameters

Quality of the ADed films is dependent on several operation parameters as well as materials properties. All of them are equally important and therefore will be discussed.

3.1. Operation parameters

Numerous experimental parameters control quality of the ADed films. Among these processing parameters, carrier gas, gas pressure in aerosol chamber and deposition chamber, gas flow, stand-off distance between the nozzle and the substrate, and the scan speed are believed to be most important. Table 2 collects some useful information on the parameters used.

It is commonly recognized that gas flow is one of very important parameters since the velocity of the particles is determined by the speed of the gas and gas pressures [38,39]. Difference in the pressure between deposition chamber and aerosol chamber influences the adhesion of particles and substrate [40]. It was noted that the type of the carrier gas may also affect the morphology of ADed films. For example, the roughness and thickness an ADed Si film using a He gas is much larger than that through using Ar as a carrier gas [41]. It was also found that using He as a carrier gas would double the particle velocity than that using air [42]. Nevertheless, the stand-off distance between nozzle and substrate can seriously modify the morphology of the film, and this tendency is amplified with the carrier gas flow increase [43]. Although it was also noted that angle between nozzle and substrate also affects the deposition efficiency and properties of film, there is no summary of this parameter because the research in this parameter is limited [44]. The hardness of powder and substrate material and roughness of substrate surface strongly affect the interface quality and the interlayer bonding of the ADed layer [45]. The influence of materials properties will be illustrated detailly in the next section.

3.2. Pre-heat treatment of powder and post-heat treatment of film

Pre-heat treatment of raw powder or post-heat treatment of film could be added into the AD process to adjust the mechanical properties of the ADed film [60,61]. The crystallite size of particles is increased during the pre-heat treatment at appropriate temperature, which promote the fracturing and adhesion of particles [62]. Cracks of particles must run through their crystallites, as only in this case fresh and unsaturated surfaces can be formed leading to the growth and densification of ADed film. This detailed mechanism will be illustrated in the next section.

The post-heat treatment of the film after AD may engineer microstructure as well as crystallographic structure, and hence mechanical and functional properties of the films [63]. It is understood that the powder particles with large kinetic energy may cause severe deformation and defragment during the collision moment, resulting in formation of nanocrystal. A post-heat treatment may induce at least three effects, namely partial annihilation of defects, grain size, crystal structure, and adhesion of the ADed film [64,65]. Since the purpose of post-heat treatment is not for sintering, the annealing temperature is around 200–600 °C, which is much lower than conventional sintering temperature [66]. It was found that the permittivity of ADed film could be largely increased through this processing [67].

To minimize the impact of thermal annealing on substrate and interfaces, rapid annealing has usually been used such as infrared laser irradiation to suppress local thermal damage to the back sides of the lead zirconate titanate (PZT)/SUS and substrate near the film edge and to retain the dielectric and/or ferroelectric properties of the PZT/SUS [68]. Since it is able to promote the grain growth of ADed film which has been used for different applications [3,69].

4. Mechanisms of adhesion and densification

The mechanism of deposition can be divided into two stages. In the first stage of AD, the powder particles collide and adhere to form an anchor layer on the surface of substrate creating a bonding between the particles and the substrate. This stage is important since it determines whether the powder can produce a film on this substrate successfully. In the second stage, the particles continuously deposit on the anchor layer. By repeating this process through layer-by-layer, finally a thick film is thus formed. The second stage is crucial for controlling the thickness of ADed film.

4.1. Collision and adhesion phenomena

Since AD is simply a collision process, the composition of the ADed film remains unchanged from results of X-ray diffraction (XRD) and energy dispersive X-ray spectroscopy (EDS) as shown in Fig. 6(a) and (b).

Table 2
Parameters in Aerosol deposition (AD) method from previous works.

Ref	Materials	Substrate	Thickness	Pressure in deposition chamber	Pressure in aerosol chamber	Carrier gas	Gas flow	Nozzle geometry	Scanning rate	Distance between nozzle and substrate	Particle size	Operation time
[25]	Sn_4P_3/C	Stainless steel (SUS316L)		20 Pa		N_2	20 L/min	10 mm * 0.5 mm	2	10 mm	0.5–1.5 μm	20–30 min
[46]	Fe_2O_3	SUS	0.3 μm and 1.7 μm			dried air	20 L/min	25 mm * 0.8 mm			0.5 μm	
[47]	C-coated $LiFePO_4$	SUS	1 μm			dried air	20 L/min	25 mm * 0.8 mm				
[47]	Graphite	SUS	250 nm			dried air	20 L/min	25 mm * 0.8 mm				
[48]	$LiFePO_4$/C	SUS304	745 nm	10 torr		O_2	$5*10^{-4}$ m3/s	100 mm * 0.8 mm			300 nm	5 min
[26]	$Li_{1.5}Al_{0.5}Ge_{1.5}(PO4)_3$ (LAGP)	SUS316L	10 μm	10 Pa		N_2	20 L/min	10 mm * 0.5 mm		10 mm	0.5–1 μm	20 min
[49]	$LiNi_{1/3}Co_{1/3}Mn_{1/3}O_2$ (NMC)	Li^+-conductive glass-ceramic sheets	7 μm	$4\text{-}8*10^3$ Pa		Ar	10 L/min	10 mm*0.23 mm	50 mm/ min			40 min
[50]	$Al_{0.2}Li_{6.025}La_3Zr_{1.625}Ta_{0.375}O_{12}$ (ALLZTO)	Cu	30 μm			N_2; O_2	8 L/min; 4 L/min	25 mm * 0.4 mm	1 mm/s	3 mm	8 μm	
[51]	$Li_{1.3}Al_{0.3}Ti_{1.7}(PO_4)_3$ (LATP)	SUS	3–5 μm	20 Pa before deposition and was kept constant at 120 Pa		He	5 L/min	4 mm^2			1 μm	
[52]	Cu coated on Si	Cu		8 pa							4 μm 0.035 mg	
[40]	Mg_2Ge	Cu	3,7 μm	2 pa	$8*10^5$ pa	Ar		D = 10		10 mm	0.5–3 m.	
[53]	$Li_4Ti_5O_{12}$	SUS	3.0–3.3 μm(0.42 mg)	10 pa		N_2	20 L/min	10 mm * 0.5 mm		10 mm	5−6 μm	20 min
[54]	SnO	Cu	80–100 μg	several ten Pa	$7*10^5$pa	Ar		D = 0.8				
[55]	Sn_4P_3	SUS		20−30 Pa		N_2	10 L/min	10 mm * 0.5 mm	10 mm/s	10 mm		10 min
[56]	$Na_2Zn_2TeO_6$ (NZTO)	SUS	25 μm	50 pa		Ni	10 L/min	10 mm * 0.5 mm	10 mm/s	10 mm		10 min
[57]	$Li_{0.35}La_{0.55}TiO_3$ (LLT)	SUS	10–20 μm					35 mm * 0.8 mm				
[58]	LiV_3O_8 (LVO)	$Li_7La_3Zr_2O_{12}$ (LLZO)		20 Pa		N2	20 L/min	10 mm * 0.5 mm	10 mm/s	10 mm	0.5–2 μm	5–10 min
[27]	$LiCoO_2$(LCO)	LLZO	15 μm			Ar	15 L/min	0.1 mm * 10 mm	600 mm/ min		2.2 μm	
[59]	$LiNi_{1/3}Co_{1/3}Mn_{1/3}O_2$ (NCM) + LATP	LLZO	20 μm	3–5 Pa/$8*10^2$ Pa		Ar	10 L/min	10 mm * 0.23 mm	50 mm/ min		10 μm	
Summary [2]				0.2–20 mbar	60–1066 mbar	Air, N_2, O_2, Ar, H2	1 L/min - 30 L/min	10 mm*0.5 m to 35 mm*0.8 mm	0.05–10 mm/s	0.5–50 mm	200 nm-5 μm	

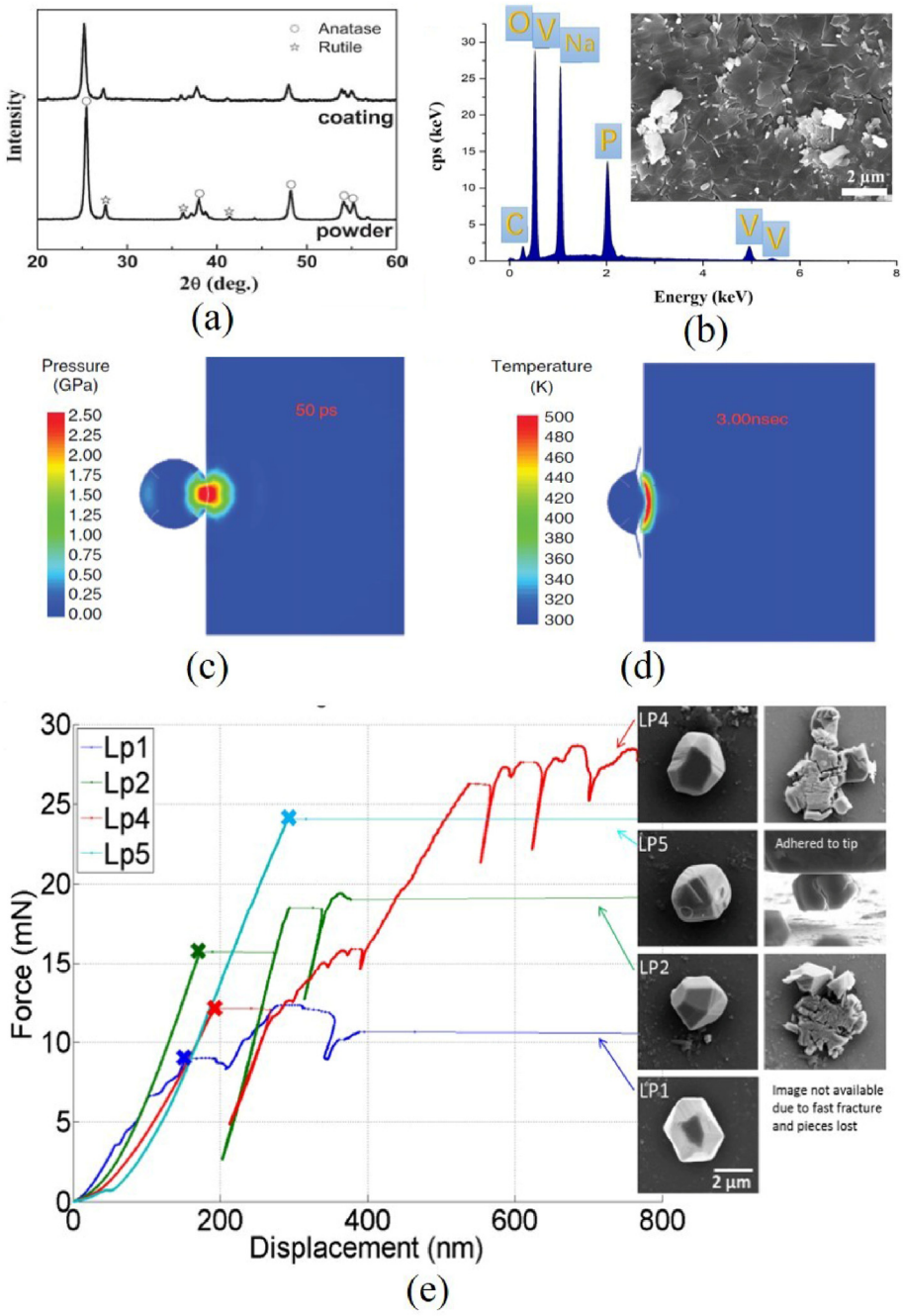

Fig. 6. (a) XRD pattens of ADed film and raw powder [69], (b) EDS results of $Na_3V_2(PO_4)_3$ ADed film [70], (c) finite-element method simulation of the shock pressure, (d) changes of local temperature by impact of particle with the substrate [71], and (e) load vs. displacement curves as well as SEM images before and after loading for four 3 μm particles (LP1, LP2, LP4, and LP5) [75].

Since AD is operated at room temperature and no thermal energy is provided, there will be no thermally driven diffusion, which is also reflected by the XRD spectra [70,71]. According to results of experiments and simulations from several works, it is proved that no melting occurs during collision. For example, the shock pressure at the impact area and maximum local temperature on the spots of collision do not exceed 10 GPa (Fig. 6 (c)) and 500 °C (Fig. 6 (d)), respectively, assuming the velocity of the α-Al_2O_3 particles is about 300 m s^{-1} which was gotten from experiments. This temperature is much lower than the melting point of Al_2O_3. So, it is obvious that the adhesion of the film is not caused by chemical reaction or melting but by mechanical bonding [72].

Since kinetic energy of particles is one of the key parameters in AD process, understanding the flying speed of the particles during deposition and hence adjust the parameters become critical in AD. Particle image velocimetry (PIV) [34], the time-of-flight method (TFM) and impact-pressure method (IPM) are therefore used for investigating the velocity of solid particles in the AD [73,74]. It has been noted from the measurements that the velocities of the particles are in the range from 200 to 600 m s^{-1} which agrees with simulation results of gas flow velocity at the exit of a nozzle.

The computational fluid dynamics simulation (CFD) is used to simulate the possible flight path of particles with various sizes, enabling a probabilistic sense to demonstrate how the majority of particles impact on to the substrate. The simulation results suggest that clumps of particles are effectively broken up during impact on substrate [75]. In-situ micro-compressions in SEM and TEM which simulate collision of

particles on a substrate provides some useful information on the bonding mechanism between the particles and the substrate (Fig. 6(e)), suggesting that the bonding mechanism is through plastic deformation and fracture of particles under applied compression [76]. It is proved that single ceramic particle can be plasticly deformed when it hits on the substrate in AD process. It is also noted that the degree of mobile dislocations will be accommodated depending on the kinetics of the particles in AD.

The crystallite size of the ADed film compared with the grain size of the original particles was largely reduced during impacting from 1 μm to a few tens of nanometer. Fig. 7(a) through 7(b) show the SEM images of the raw powder and the ADed films [72]. It is obvious that the crystallite size of the ADed film is smaller than that of the raw particle size, which is also estimated by the full width at half of maximum intensity of the XRD measurement. The orientation of the ADed film depends more on anisotropy of chemical bonding than the anisotropy of particle shapes of raw powders [70]. All the examples above provide the evidence of particles' fracture in consolidation of deposition.

The mechanical bonding between particles and the substrate as well as between particles and particles of the ADed film was further characterized by transmission electron microscopy (TEM) with assistance of focused ion beam (FIB). It was observed that the particles were broken into "splat" to form anchor layer when impacting on substrate with high hardness in Fig. 7(d)I [77]. The dislocations of substrate under the surface should be caused by particle impacting and bouncing off which can be observed in Fig. 7(d)I. The interfaces of particle-substrate and particle-particle were scrutinized by TEM at different magnification which are showed in Fig. 7(d) II-IV. It is clear that the sound bonding appeared in the middle region of interface of splatted particle and substrate. Meanwhile, there is obvious gap between the edge of splatted particle and substrate. When at higher magnification, a small layer of disorder phase was investigated in the interface of bonded region. This proved the mechanical bonding in the interface and deformation of substrate are due to the high kinetic energy of particles.

Study has shown that formation of the anchor layer is also influenced by the relative hardness ratio between the particle and the substrate. For example, it was observed that the particles were broken into "splat" to form anchor layer when impacting on substrate with high hardness [77]. Otherwise, the formation of the anchor layer is a bit different at a faster rate on a substrate with low hardness such as Cu metal substrate [78]. When hard ceramic powder is used, such as alumina, due to its high hardness and strength, the particles will not be plastically deformed, and instead the anchor layer will be formed via denting the Cu surface upon impact of the alumina particles onto the surface and the particles embed into the soft substrate (Fig. 7(c)). Microstructure characterization reveals that the grain sizes on the top layer of a film is much smaller than that at

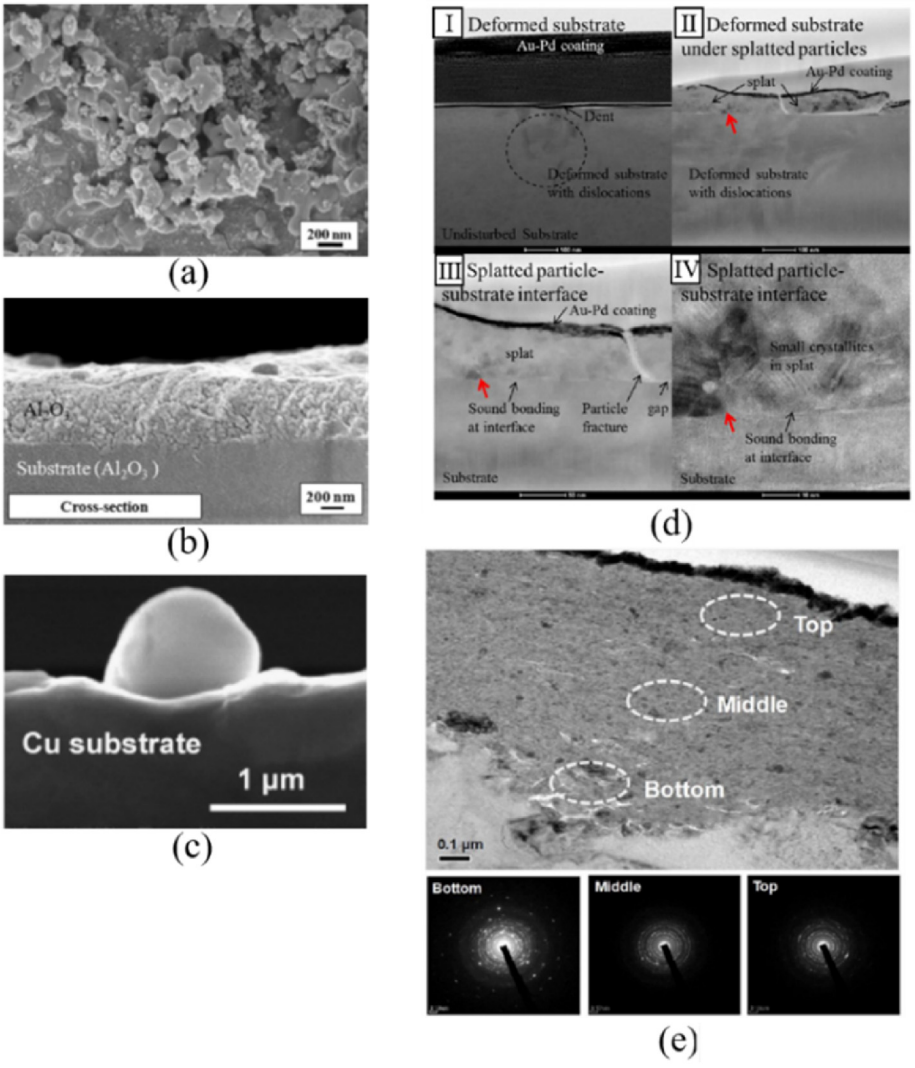

Fig. 7. SEM images: (a) raw particles, (b) cross-section of ADed film [72] and (c) a-Al_2O_3 particle embedded in Cu substrate [78]; Cross-sectional TEM images: (d) interface of particles-substrate [42], and (e) three regions (bottom, middle, top) of the ADed film [79].

the bottom region of the film if a soft substrate is used, indicating less deformation and fragment of the particle since large amount kinetic energy of the particles is absorbed by the soft substrate. This phenomenon is called "cushioning effect" of the ductile substrate due to the difference between the mechanical properties of the ductile substrate and hard particle [79]. As a result, the porous layer containing voids formed near the soft substrate as shown in Fig. 7(e) providing the possibility for fabricating the flexible electronic devices.

Based on all observations, it can be concluded that to achieve good adhesion and anchor layer, particles with sub-micro size, hardness, microstructure, and substrate are critical, and velocity prior collision. During the extremely short period of collision, most of the kinetic energy of particles is absorbed by severe plastic deformation and fracture of particles, some of it is dissipated as heat, and small portion is stored in the particles as strain energy. Furthermore, the substrate is also subjected to deformation particularly during formation of the anchor layer. The mechanochemical bonding might also be possible at the interface of the middle area of "splat" and substrate which is similar to grain boundaries. At the same time, the particles might embed into the soft substate to form anchor layer. Although there are small gaps between substrate and edges of particles, the bonding between anchor layer and substrate would be strengthened in the subsequent deposition process.

4.2. Consolidation and growth of ADed film

A thick film is made by repeated deposition layer-by-layer similar to a 3D printing process. Therefore, the interaction of particles between layers plays a significant role in formation of a film and adhesion [75]. In the stage of consolidation and growth of ADed film, particles continue to collide on to the anchor layer at a velocity in the range of critical velocities, providing the similar conversion of energy, deformation, and mechanochemical bonding. In addition, the subsequent particles collide on to the edges of previous "splat", leading to strengthening the bonding between previous particles of the layer and the substrate, which is schematically shown in Fig. 8(a). The kinetic energy of subsequent particles is not only used for deformation and converted into bonding energy, but also for compaction of the previous layers of particles, reinforcing the particle-particle bonding. This phenomenon is termed as "tamping effect" or "hammering effect" that is the crucial effect for formation of ADed film with dense structure and great adhesion to the substrate [80]. The higher particle velocity, the stronger tamping effect, achieving a compact bonding between particle and particle, and between particle and substrate. These processes are repeated layer-by-layer until a targeted thick and dense ADed film is formed.

So far, the fundamentals of consolidation mechanism of the ADed film are still in the exploration stage. Some researchers are trying to explain it by mechanical bonding mechanism of particle-particle and particle-substrate through simulation and characterization of the ADed film.

4.3. Requirements for materials

The success of bonding between particles and substrate as well as between particles themselves is significantly influenced by particles' behaviors. Therefore, precise control of the raw material's features is essential, such as particle distribution size, shape, density, hardness, macro-defect density, and microstructure.

It has been noted that only particles of a right size and size distribution can be deposited properly on the substrate at the right velocity. The particle size in range between 200 nm and 5 μm can be accelerated by proper gas flow to around 200–600 m s^{-1}. The kinetic energy density for particles is estimated to be 79–711 MJ/m^3, assuming that a little kinetic energy is lost to thermal energy at impact while the majority of kinetic energy is transferred to deformation energy [76]. Fig. 9 shows the different phenomena when the particles within different size collide on the substrate. With sufficient high kinetic velocity, suitable-sized particles would be able to withstand the high deformation energy associated with dislocation plasticity (without fracture) and to achieve the adherence to the substrate. However, for tiny particles, they may be elastically bounced back when colliding to the substrate. For too large particles, they may be fractured at a high kinetic energy during the collision. In the interim, the large particles may abrasively blast and scrap the surface of the substrate. Additionally, agglomeration of particles is a significant issue for film densification which is often encountered and tremendously affects quality of the ADed film as well as the deposition efficiency. Agglomeration of nanoparticle that is typically caused by van der Waals forces, static electronical forces, and moisture has a big issue since the kinetic energy will be consumed for breaking the agglomeration instead of being transferred into bonding energy [81].

Shape and microstructural features of the particles also affect film properties [82]. For example, The ball-milled and heat-treated powder which has polycrystalline structures formed by partially aligned dislocations exhibited higher deposition efficiency due to its increased plastic deformability [83]. The thickness and grain orientation of the ADed film is influenced by particles' shape by comparison of the same composition particles in different shape, such as, sphere, plate-like and angular [84]. According to the results from Langevin dynamics simulations monodisperse, polydisperse, aggregated, and coalescing particles, the pore size distribution modes in ADed films is near or above the primary particle geometric mean radius [85].

It is crucial to produce the suitable size and shape of the particles to

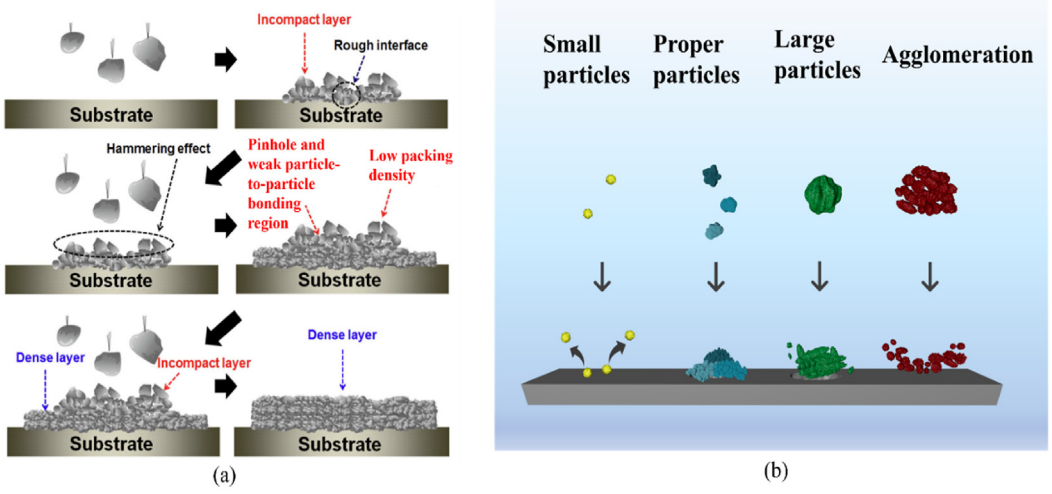

Fig. 8. (a) Schematic diagram of the densification procedure of ADed films [79] and (b) impact phenomenon of particles in different size.

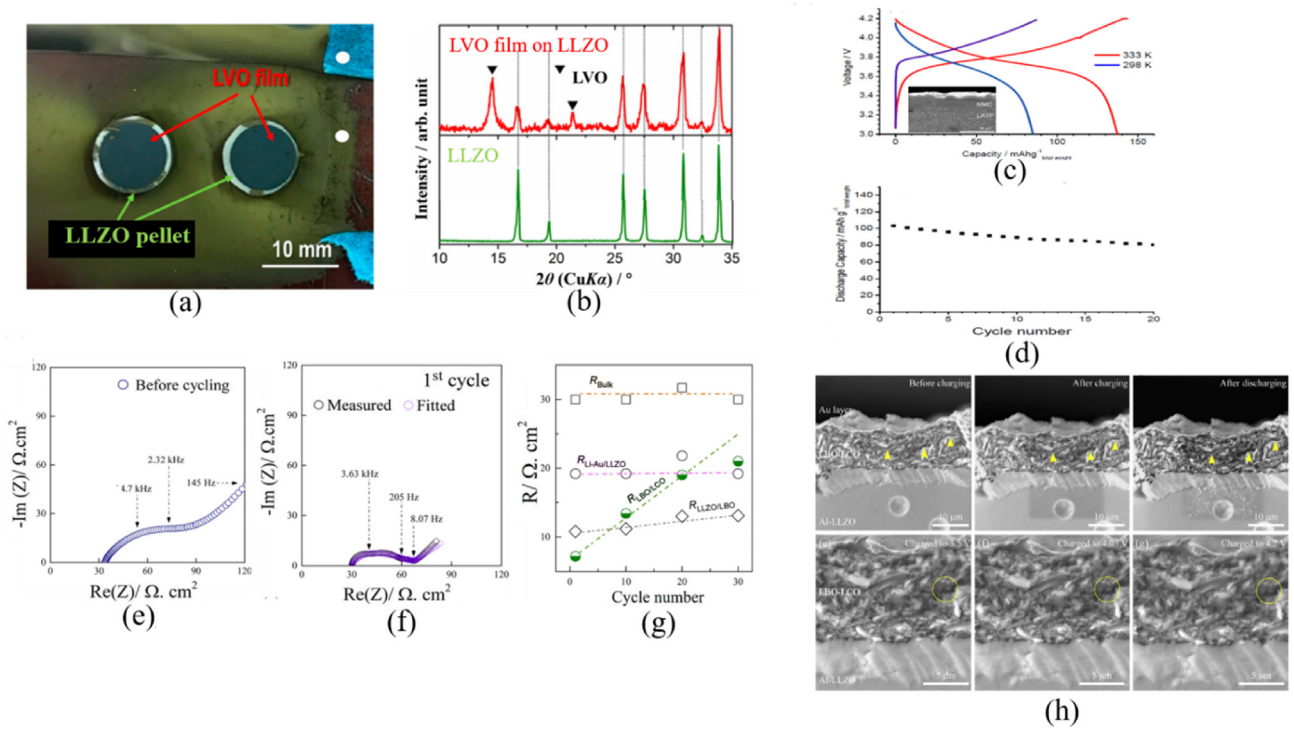

Fig. 9. (a) Image and (b) XRD spectra of the LVO film on a Ta-doped $Li_7La_3Zr_2O_{12}$ (LLZO) pellet by AD [57], (c) initial charge-discharge curves and (d) cycle performances of ASSB (Li/LiPON/LATP-sheet/NMC-composite-film by the NMC-30/Pt). The inset shows the cross-sectional SEM image around the composite film electrode/LATP-sheet interface [48], EIS of the Li–Au | LLZO | ADed LBO-LCO cell (e) before cycling, (f) during 1st charging and (g) evolution of the resistance components with cycling, and (h) in-situ SEM analysis of the degradation mechanism of the Li–Au | LLZO | ADed LBO-LCO [110].

avoid agglomeration. Ball milling, pre-heat treatment and sieving method have been used to control the particles' properties in some studies [86]. Controlling the size and shape of particles is believed to be effective for increasing the deposition efficiency and obtaining high quality films.

5. Applications of AD in batteries

Nowadays, battery is playing an important role in daily life, especially in the mobile electronic devices and electrical vehicles. However, it also faces various tough challenges such as capacity, cyclicity, and safety issues. The AD has been explored for a variety of applications to overcome these issues, including as a method for depositing solid-state electrolyte (SSE), cathode and anode materials, and current collectors.

In the processing of deposition of the cathode and anode electrodes, it has shown promise in producing high-quality cathode electrodes with improved electrochemical performance and stability. On the other hand, the AD shows more possibility in the production of ASSBs which are considered as the candidate to solve the safety issue of batteries. Not only it can deposit the thin film electrolyte with high quality but also it is able to integrate other battery components with solid-state electrolyte for the development of high-performance and long-lasting ASSBs.

5.1. Deposition of electrodes

It is still challenging to develop a high-capacity electrode where ions can intercalate/(de)intercalate at a fast rate with good cyclic stability. To understand the difference between the electrodes used in current rechargeable batteries and ASSBs. Let's first look at the way of preparation of conventional electrodes. The conventional preparation of electrodes is mainly based on the slurry-casting method, in which the active materials, conductive carbon and nonconductive binders are mixed into a slurry form which is then cast on aluminum or copper foil [87]. In this process, conductive carbon provides an electrical contact between the active materials and current collectors. The binders are used to integrate the individuals of active materials, conductive additives, and current collectors [88]. Regrettably, the binders are generally insulating and electrochemically inactive, which not only decreases the electrical conductivity but also has some side effects with the electrolyte [89,90]. Both conductive carbon and binder are not ion conductive but the liquid electrolytes that penetrate into the electrodes providing good channel for ion conduction. AD provides the possibility to alter the composition of electrodes which can deposit the active materials on current collector without additives [91].

From deposition point of view, AD shows great potential in electrode manufacture which could fabricate the electrode without thermal treatment and additives. On the current collector or SSE, it can quickly deposit the powdered electrode active ingredients. Additionally, the ADed electrode has stronger adherence to the substrate than an electrode made by conventional method using carbon and binders [25]. Strong adhesion would prevent active materials from falling off during charge and discharge cycles, improving cyclic stability. Table 3 tabulates some earlier works of the ADed electrodes being employed with liquid and polymer electrolytes.

The alloy-based anode fabricated by the AD shows better electrochemical properties due to high electronic mobility [55]. For example, the capacity retention of the ADed Sn_4P_3 electrode in a cell with a polymer electrolyte was much better than that in a cell with a liquid electrolyte after galvanostatic cycling. It might be attributed to a reduced microstructural change of the ADed film and no side effect with polymer electrolyte after galvanostatic cycling with polymer electrolyte.

Meanwhile, electrodes fabricated by AD also meets some problems. Although the ADed film has the similar structure and physical properties as its raw powder, the crystallite size of the ADed film is smaller than the particle size before deposition, which may affect the electrochemical performance [3]. The ADed film has a strong mechanical bonding with

Table 3
Summary of the previous studies about cases of ADed electrode.

ref	category	deposited materials	cathode	anode	electrolyte	capacity	stability	comment
[25]	anode	tin phosphide–carbon (Sn_4P_3/C) composite film on ss	Li	Sn_4P_3/C	liquid	1000 mAh/g (theoretical gravimetric capacity = 1255 mAh/g)	700 mAh/g after 100 cycles; 380 mAh/g even after 400 cycles	
[47]	cathode	C-coated $LiFePO_4$	C-coated $LiFePO_4$	Li	liquid	14 μAh/cm^2 at 1 μA/cm^2, 158 mAh/g	50 cycles	
[47]	cathode	graphite	Li	graphite	liquid	22 μAh/cm^2	50 cycles	good cycle performances are observed at 1 and 50 μA/cm^2
[48]	cathode and anode	$LiFePO_4$/C	$LiFePO_4$/C	Li	liquid	31 mAh/cm^2	50 cycles	poor rate capability at 0.2 and 2C rates
[52]	anode	Cu coated on Si	Li	Cu coated on Si	liquid	870 mAh/g	61 % 1000cycyles	
[40]	anode	Mg_2Ge	Li	Mg_2Ge	liquid	95 mAh/g	35 % 200cycles	
[93]	anode	Mg_2Ge/Si	Li	Mg_2Ge/Si	liquid	1200 mAh/g	50 % 200 cycles.	
[94]	anode	Ru coated on Si	Li	Ru coated on Si	liquid	1500 mAh/g	39 % 1000cycyles	
[26]	anode	$Li_4Ti_5O_{12}$	Li	$Li_4Ti_5O_{12}$	liquid	159 mAh/g (0.5C); 125 mAh/g(20C)	98 % 100 cycles (1C)	
[95]	anode	Ni–P coated	Li	Ni-coated	liquid	1590 mAh/g	50 % 1000cycyles	
[54]	anode	SnO	Li	SnO	liquid	580 mAh/g (0.07C)	43 % 50 cycles	
[91]	cathode	$LiNi_{0.4}Co_{0.3}Mn_{0.3}O_2$ (NCM)	$LiNi_{0.4}Co_{0.3}Mn_{0.3}O_2$ (NCM)	Li	liquid	44.7 μAh/cm^2	43.5 μAh/cm 2cycles	
[46]	cathode	Fe_2O_3	Fe_2O_3	Li	liquid	150 mAh/cm^2		Thicker, better rate performance
[95]	cathode	$Na_3V_2(PO_4)_3$	$Na_3V_2(PO_4)_3$	Na	liquid	32.2 mAh/cm^2	88.6 % 1000 cycles	
[96]	cathode	LiNi0.5Mn1.5O4 (LNM)-LATP composite	LNM-LATP composite	Li	lithium phosphorus oxynitride glass(LiPON)	6.8 mAh/g (100C)	3.7 mAh/g for 21st-25th cycles (100 °C)	500 °C annealing; graphite film between Li and LiPON
[55]	anode	Sn_4P_3	Li	Sn_4P_3	polymer	900 mAh/g	78 % 75 cycles	420 mAh/g liquid electrolyte

current collector or with SSE, which may result in large interface stresses. Due to poor electric as well as ionic conductivity, the thickness and mass load of the electrodes is limited [46]. To address these issues associated to electric conductivity and ion transportation in the electrode, the active powder particles can be lightly coated a layer of carbon or incorporated with small amount of electrolyte [92].

5.2. Electrolytes

Solving the safety problems is one of the main objectives of the next generation battery. SSE is a good substantial for organic liquid electrolyte to reduce the safety risk of batteries [97]. There are several kinds of solid-state electrolytes used to create the ASSBs. including Oxide- [98], phosphate- [99,100] and polymer-based electrolytes [101].

SSE thin film with low thickness can achieve better conducting properties. It can also be used in micro-device and increase the volumetric energy density. Table 4 shows the conductivity of electrolyte thin films fabricated by AD. Although the ionic conductivity of ADed film electrolyte is more than one order of magnitude lower than that of sintered electrolyte by conventional method, it still has a lower total resistance value due to the small thickness.

5.3. All-solid-state battery

Since ASSB employ nonflammable SSE to replace the organic liquid electrolyte, the safety concern of battery can be largely reduced [103,104]. However, the interface between electrode and electrolyte in ASSB is solid-solid, which is very different from the liquid-solid in the traditional battery, leading to another issue. Normally, for the traditional cells, the surface of the electrode is wetted with liquid electrolyte and the additional electrolyte infiltrates into the active materials, resulting in a good contact for charge carriers' transportation, whereas the SSE has a rigid interface with electrode particles at point-to-point contacts limiting the ion transport [105]. The volume change of the electrode during electrochemical cycling may also cause damage to these rigid connects, restricting ion conduction and electrochemical response in the electrode [103]. How to produce a striking interface between the electrode and the SSE hence becomes a key to improve the electrochemical performance of ASSB. Fabrication of battery through AD may provide a solution to directly integrate the thick electrode film on to the SSE or the electrode and electrolyte layer-by-layer, which is not only cost-effective but also of high quality in comparison with other deposition technologies such as PLD [106,107], CVD [108], plasma spraying [109], and ion-beam deposition [110]. As stated before, AD process is a room temperature operation. This heating-free and binder-free process enable to eliminate the mismatch of thermal stability of both electrodes and solid electrolytes, and reduces the likelihood of undesired side reactions (e.g. mutual diffusion layers) between the materials [59]. Some studies although limited are summarized in Table 5.

Table 4
Summary of the previous studies about cases of ADed electrolyte.

Ref	materials	substrate	conductivity
[26]	$Li_{1.5}Al_{0.5}Ge_{1.5}(PO_4)_3$ (LAGP)	Stainless steel (SUS)	0.5*10^{-5} S/cm
[50]	$Al_{0.2}Li_{6.025}La_3Zr_{1.625}Ta_{0.375}O_{12}$ (ALLZTO)	Cu	4.7 *10^{-5}(23 °C); 3.1 *10^{-4}(70 °C) S/cm
[51]	$Li_{1.3}Al_{0.3}Ti_{1.7}(PO_4)_3$ (LATP)	SUS	1.12*10^{-6} S/cm
[56]	$Na_2Zn_2TeO_6$ (NZTO)	SUS	0.74 *10^{-5} S/cm
[57]	$Li_{0.35}La_{0.55}TiO_3$ (LLTO)	SUS	6.38 * 10^{-7} S/cm
[102]	$Li_7La_3Zr_2O_{12}$ (LLZO)	AL	7 * 10^{-5} S/cm

Table 5
Summary of ASSBs fabricated by AD.

ref	category	deposited materials	substrate	cathode	anode	electrolyte	capacity	stability	comments
[49]	Cathode	$LiNi_{1/3}Co_{1/3}Mn_{1/3}O_2$ (NCM)	LATP	NCM	Li	LATP-LiPON	87 mAh/g (298 K); 138 mAh/g (333 K)	over 20 cycles	Li/LiPON/LATP-sheet/NMC-composite-film/Pt
[58]	Cathode	LiV_3O_8 (LVO)	$Li_7La_3Zr_2O_{12}$ (LLZO)	LVO	Li	LLZO	100 mAh/g (50 °C) 290 mAh/g (100 °C)	150 mAh/g (100 °C) 35 cycles	
[111]	Cathode	Li_3BO_3 (LBO)-$LiCoO_2$ (LCO)	ALLLZO	LBO-LCO	Li	ALLLZO	128 mAh/g (60 °C)	87 % 30 cycles	
[27]	Cathode	LCO	LATP	LCO	Li	LATP	70 mAh/g (100 °C)		350C annealing
[59]	Cathode	NMC + LATP	LLZO	NMC + LATP	Li	LLZO	135 mAh/g	90 % 90 cycles (100 °C)	
[96]	cathode	$LiNi_{0.5}Mn_{1.5}O_4$ (LNM)-LATP composite	LNM-LATP composite	LNM	Li	LATP-lithium phosphorus oxynitride glass electrolyte (LiPON)	6.8 mAh/g for 1st-5th	stable over 90 cycles 100 °C	500 °C annealing
[113]	Cathode-electrolyte	$LiFePO_4$ (LFP)-LLZO	SUS	LFP	Li	LLZO	19 μAh/cm^2, 53 mAh/g (0.3C)	90 cycles (100 °C)	$1 * 10^{-8}$ S/cm at 140 °C

Fig. 9(a) shows an example of LiV_3O_8 (LVO) electrode on $Li_7La_3Zr_2O_{12}$ (LLZO) substrate by AD. XRD results of this AD sample are shown in Fig. 9(b) revealing no side effect after the AD with the perfect match of LLZO before and after AD. The initial charge-discharge curves and cycle performances of ASSB fabricated by AD are shown in Fig. 9(c) and (d). The insert SEM image shows the monothetic interface between electrode and electrolyte by AD. In this ASSB fabricated by AD, the stable charge-discharge reactions with thick composite cathode films, $LiNi_{1/3}Co_{1/3}Mn_{1/3}O_2$ (NMC) are ascribed to the incorporation of glass-ceramics solid electrolyte, Li–Nb–O in the composite films. 3D-nano-network amorphous solid-state electrolyte (Li–Nb–O) coating on NCM is an important parameter for the dense composite film formation on the solid-state electrolyte substrate $Li_{1.3}Al_{0.3}Ti_2(PO_4)_3$ (LATP). In addition, the LiPON is used to prevent the direct reactions between LATP and Li metal. So the complete construction of this ASSB fabricated by AD is Li | LiPON | LATP-sheet | NMC-LiNbO composite-film | Pt.

The degradation mechanism of ASSBs (Li–Au | LLZO | ADed Li_3BO_3 (LBO)- $LiCoO_2$ (LCO)) fabricated by AD has been studied by electrochemical impedance spectroscopy (EIS) and in-situ SEM [111]. The Nyquist plots of this ASSB before cycling and after the 1st charging-discharging process, are shown in Fig. 9(e) and (f) respectively. It was proved that the interfacial contact between electrode (ADed LBO-LCO) and SSE (LLZO) was improved after the initial charging process through the comparison of EIS results of cells before cycling and after 1st cycle charging. In addition, three poorly resolved arcs are observed in the frequency domain from 3 MHz to 8 Hz, which can be assigned to the three types of interfacial resistance including $R_{Li-Au\ |\ LLZO}$, $R_{LLZO\ |\ LBO}$ and $R_{LBO\text{-}LCO}$ But the total resistance increased with cycling, which was very likely related to the electromechanical degradation of the LBO-LCO interface, caused by the insertion and extraction of Li ions into and from LCO, which are summarized in Fig. 9(g). In-situ SEM results shown in Fig. 9(h) was performed to verify the proposed crack evolution mechanism in LBO-LCO leading to the degradation of this ASSB. The pre-existing cracks become larger and deeper after the initial charging and discharging, as indicated by the arrowheads in Fig. 9(h).

Annealing at appropriate temperature after deposition could recover the crystallite defects and significantly reduce the interfacial resistance. STEM-EELS spectrum imaging verified interfacial resistance was reduced after thermal annealing at 250−300 °C, but the interfacial resistance was increased after thermal annealing at 400 °C, attribute to the formation of a Co_3O_4-like spinel blocking layer at the electrolyte and electrode interface (LATP | LCO) [112].

5.4. Others

In addition to ASSB, AD can also be used in fields of solar cells, fuel cells and flexible batteries. High-temperature solid oxide fuel cells (SOFCs) generate energy through the recombination of hydrogen and oxygen. They need a diffusion barrier layer between the electrolyte and cathode to prevent of cell aging during operating at high temperature. A diffusion barrier film with good adhesive can be deposited on solid state electrolyte by AD method [114,115]. A compact and porous TiO_2 ADed film was used in dye-sensitized solar cells (DSSCs) which enhanced the conversion efficiency [116]. Active materials also can be deposited on ductile substrate to achieve flexible batteries by this method [79,117].

6. Challenges and perspectives

As a room temperature processing, AD is capable to deposit different materials on various substrates. Since AD directly deposits powder particles onto previous layer or substrate, the rate of deposition is much faster than other physical deposition. By understanding operation of the AD machine and mechanisms of this cold collision at extremely high kinetic energy, the operating parameters can be finally optimized. Since it is a room temperature process, the interface will be clean from interfacial diffusion. However, there still exist a number of challenges before being truly industrially exploited.

(a) Current study of AD for ASSBs is still based on a single line/belt deposition. For a large area deposition, deposition through line-by-line is necessary, which may cause concern of pitching between different deposition lines.
(b) Charge transfer on the interface in ASSB requires two essential conditions, namely electrons and ions transportation. Therefore, the electrode must contain additional material(s) which can conduct electron as well as ions. Although AD is able to deposit carbon-coated active materials, increase in ionic conductivity of the electrode becomes a bottle neck. The simultaneous co-deposition of electrode material and electrolyte particles may solve this problem after seeking out the proper operation parameters. Interfacial investigations hold a crucial role in both AD technology and the realm of batteries. The in-situ characterization of batteries, included in-situ XRD and in-situ TEM, may provide more useful information for further interfacial studies and generate new idea for interfacial studies of ADed films.
(c) Suitable manufacturing process for ASSBs is still unclear leading to difficulty in determine if ASSBs should be processed layer-by-layer or layered on preprepared solid electrolyte. Therefore, system design and optimization are essential for overcoming the manufacturing hurdles associated with ASSBs and paving the way for the successful industrial applications.

(d) AD parameters are machine and materials dependent and suitable AD machines should be designed. The optimized parameters for one type of AD machine cannot be directly adapted by another type of machine.

Overall, AD is a promising processing for battery. From recent successful research works and data, it can be not only used for the processing ASSBs but also for fabricating electrode sheets for current batteries since it entirely removes insulating binder. Therefore the technology is worth exploring further.

Declaration of competing interest

Li Lu is an editorial board member for [Nano Materials Science] and was not involved in the editorial review or the decision to publish this article. All authors declare that there are no competing interests.

Acknowledgements

This work was supported by National University of Singapore (Chongqing) Research Institute, National University of Singapore, Chongqing Postdoctoral Research Special Funding, Overseas Postdoctoral Research Start-up Funding, and Natural Science Foundation of Chongqing, China (cstc2021jcyj-msxmX0086).

References

[1] M.N. Rahaman, Ceramic Processing and Sintering, CRC press, 2017.
[2] D. Hanft, J. Exner, M. Schubert, T. Stöcker, P. Fuierer, R. Moos, J. Ceram. Sci. Technol. 6 (2015) 147–182.
[3] J. Akedo, M. Lebedev, Jpn. J. Appl. Phys. 38 (1999) 5397.
[4] J. Akedo, Mater. Sci. Forum 449–452 (2004) 43–48.
[5] S. Kashu, E. Fuchita, T. Manabe, C. Hayashi, Jpn. J. Appl. Phys. 23 (1984) L910.
[6] A. Hariz, A. Schroth, M. Ichiki, R. Maeda, J. Akedo, V.K. Varadan, O. Reinhold, in: Smart Electronics and MEMS, 1997, pp. 380–387.
[7] N. Izyumskaya, Y.I. Alivov, S.J. Cho, H. Morkoç, H. Lee, Y.S. Kang, Crit. Rev. Solid State Mater. Sci. 32 (2007) 111–202.
[8] M. Ichiki, J. Akedo, A.S.A. Schroth, R.M.R. Maeda, Y.I.Y. Ishikawa, Jpn. J. Appl. Phys. 36 (1997) 5815.
[9] J. Akedo, J. Am. Ceram. Soc. 89 (2006) 1834–1839.
[10] M. Schubert, J. Kita, C. Münch, R. Moos, Funct. Mater. Lett. (2019) 12.
[11] M. Schubert, D. Hanft, T. Nazarenus, J. Exner, M. Schubert, P. Nieke, P. Glosse, N. Leupold, J. Kita, R. Moos, Funct. Mater. Lett. (2019) 12.
[12] A. Vardelle, C. Moreau, N.J. Themelis, C. Chazelas, Plasma Chem. Plasma Process. 35 (2014) 491–509.
[13] H.-U. Krebs, M. Weisheit, J. Faupel, E. Süske, T. Scharf, C. Fuhse, M. Störmer, K. Sturm, M. Seibt, H. Kijewski, Adv. Solid State Phys. (2003) 505–518.
[14] D.H.A. Blank, M. Dekkers, G. Rijnders, J. Phys. Appl. Phys. 47 (2014).
[15] S. Reyntjens, R. Puers, J. Micromech. Microeng. 11 (2001) 287.
[16] I.P. Jain, G. Agarwal, Surf. Sci. Rep. 66 (2011) 77–172.
[17] J. Creighton, P. Ho, Chem. Vap. Depos. 2 (2001) 1–22.
[18] A. Moridi, S.M. Hassani-Gangaraj, M. Guagliano, M. Dao, Surf. Eng. 30 (2014) 369–395.
[19] W. Sun, X. Chu, H. Lan, R. Huang, J. Huang, Y. Xie, J. Huang, G. Huang, J. Therm. Spray Technol. 31 (2022) 848–865.
[20] A. Sova, V.F. Kosarev, A. Papyrin, I. Smurov, J. Therm. Spray Technol. 20 (2010) 285–291.
[21] E. Irissou, J.-G. Legoux, A.N. Ryabinin, B. Jodoin, C. Moreau, J. Therm. Spray Technol. 17 (2008) 495–516.
[22] I. Dincer, Renew. Sustain. Energy Rev. 4 (2000) 157–175.
[23] A.M. Omer, Renew. Sustain. Energy Rev. 12 (2008) 2265–2300.
[24] T. Lan, C.-L. Tsai, F. Tietz, X.-K. Wei, M. Heggen, R.E. Dunin-Borkowski, R. Wang, Y. Xiao, Q. Ma, O. Guillon, Nano Energy 65 (2019).
[25] T. Moritaka, Y. Yamashita, T. Tojo, R. Inada, Y. Sakurai, Nanomaterials (2019) 9.
[26] R. Inada, K.-i. Ishida, M. Tojo, T. Okada, T. Tojo, Y. Sakurai, Ceram. Int. 41 (2015) 11136–11142.
[27] M. Sakakura, Y. Suzuki, T. Yamamoto, Y. Yamamoto, M. Motoyama, Y. Iriyama, Energy Technol. 9 (2021) 2001059.
[28] J. Exner, M. Linz, J. Kita, R. Moos, Int. J. Appl. Ceram. Technol. 18 (2021) 2178–2196.
[29] M. Linz, J. Exner, J. Kita, F. Bühner, M. Seipenbusch, R. Moos, Coatings (2021) 11.
[30] M. Linz, J. Exner, T. Nazarenus, J. Kita, R. Moos, Open Ceramics 10 (2022).
[31] K. Mihara, T. Hoshina, H. Takeda, T. Tsurumi, J. Ceram. Soc. Jpn. 117 (2009) 868–872.
[32] C.-L. Lin, T.-H. Peng, W.-J. Wang, Powder Technol. 207 (2011) 290–295.
[33] D. Hanft, P. Glosse, S. Denneler, T. Berthold, M. Oomen, S. Kauffmann-Weiss, F. Weis, W. Häßler, B. Holzapfel, R. Moos, Materials 11 (2018) 1572.
[34] K. Naoe, M. Nishiki, A. Yumoto, J. Therm. Spray Technol. 22 (2013) 1267–1274.
[35] M.W. Lee, J.J. Park, D.Y. Kim, S.S. Yoon, H.Y. Kim, D.H. Kim, S.C. James, S. Chandra, T. Coyle, J.H. Ryu, W.H. Yoon, D.S. Park, J. Aerosol Sci. 42 (2011) 771–780.
[36] Y. Park, D.-S. Park, S.D. Johnson, W.-H. Yoon, B.-D. Hahn, J.-J. Choi, J. Ryu, J.-W. Kim, C. Park, J. Eur. Ceram. Soc. 37 (2017) 2667–2672.
[37] P. Glosse, S. Denneler, O. Stier, R. Moos, Materials (2021) 14.
[38] T.P. Mishra, R. Singh, R. Mücke, J. Malzbender, M. Bram, O. Guillon, R. Vaßen, J. Therm. Spray Technol. 30 (2020) 488–502.
[39] M. Schubert, J. Exner, R. Moos, Materials 7 (2014) 5633–5642.
[40] H. Sakaguchi, T. Toda, Y. Nagao, T. Esaka, Electrochem. Solid State Lett. 10 (2007) J146.
[41] H. Usui, Y. Kiri, H. Sakaguchi, Thin Solid Films 520 (2012) 7006–7010.
[42] P. Sarobol, M.E. Chandross, T.D. Holmes, A.S. Miller, P.G. Kotula, A.C. Hall, Sandia National Lab., SNL-NM), Albuquerque, NM (United States), 2016.
[43] M.A. Piechowiak, J. Henon, O. Durand-Panteix, G. Etchegoyen, V. Coudert, P. Marchet, F. Rossignol, J. Eur. Ceram. Soc. 34 (2014) 1063–1072.
[44] T. Shibuya, T. Mizuno, A. Iuchi, M. Hasegawa, Mater. Trans. 61 (2020) 540–547.
[45] D.-W. Lee, H.-J. Kim, Y.-N. Kim, M.-S. Jeon, S.-M. Nam, Surf. Coating. Technol. 209 (2012) 160–168.
[46] C.-W. Ahn, J.-J. Choi, J. Ryu, B.-D. Hahn, J.-W. Kim, W.-H. Yoon, J.-H. Choi, D.-S. Park, J. Power Sources 275 (2015) 336–340.
[47] C.-W. Ahn, J.-J. Choi, J. Ryu, B.-D. Hahn, J.-W. Kim, W.-H. Yoon, J.-H. Choi, D.-S. Park, Carbon 82 (2015) 135–142.
[48] I. Kim, J. Park, T.-H. Nam, K.-W. Kim, J.-H. Ahn, D.-S. Park, C. Ahn, G. Wang, H.-J. Ahn, J. Power Sources 244 (2013) 646–651.
[49] S. Iwasaki, T. Hamanaka, T. Yamakawa, W.C. West, K. Yamamoto, M. Motoyama, T. Hirayama, Y. Iriyama, J. Power Sources 272 (2014) 1086–1090.
[50] T. Nazarenus, Y. Sun, J. Exner, J. Kita, R. Moos, Energy Technol. 9 (2021).
[51] D. Popovici, H. Nagai, S. Fujishima, J. Akedo, J. Am. Ceram. Soc. 94 (2011) 3847–3850.
[52] H. Usui, H. Nishinami, T. Iida, H. Sakaguchi, Electrochemistry 78 (2010) 329–331.
[53] R. Inada, K. Shibukawa, C. Masada, Y. Nakanishi, Y. Sakurai, J. Power Sources 253 (2014) 181–186.
[54] M. Shimizu, H. Usui, H. Sakaguchi, J. Power Sources 248 (2014) 378–382.
[55] D. Azuma, R. Inada, Thin Solid Films, 2022 139537.
[56] S. Teshima, Y. Ono, N. Goto, R. Inada, Mater. Lett. 324 (2022) 132640.
[57] J.-J. Choi, C.-W. Ahn, J. Ryu, B.-D. Hahn, J.-W. Kim, W.-H. Yoon, D.-S. Park, J. Kor. Phys. Soc. 68 (2016) 12–16.
[58] R. Inada, K. Okuno, S. Kito, T. Tojo, Y. Sakurai, Materials (2018) 11.
[59] T. Kato, S. Iwasaki, Y. Ishii, M. Motoyama, W.C. West, Y. Yamamoto, Y. Iriyama, J. Power Sources 303 (2016) 65–72.
[60] D. Hanft, M. Bektas, R. Moos, Materials (2018) 11.
[61] N. Leupold, S. Denneler, G. Rieger, R. Moos, J. Therm. Spray Technol. 30 (2020) 480–487.
[62] H. Kwon, Y. Kim, H. Park, S. Jeong, C. Lee, Ceram. Int. 46 (2020) 9016–9024.
[63] Q. Yin, B. Zhu, H. Zeng, Microstructure, Property and Processing of Functional Ceramics, 2010, pp. 1–111.
[64] J. Exner, T. Nazarenus, D. Hanft, J. Kita, R. Moos, Adv. Mater. 32 (2020) e1908104.
[65] T. Nazarenus, J. Schneider, L. Hennerici, R. Moos, J. Kita, Funct. Mater. Lett. 16 (2023) 2350014.
[66] N. Leupold, M. Schubert, J. Kita, R. Moos, Funct. Mater. Lett. 11 (2018) 1850022.
[67] H. Hatono, T. Ito, K. Iwata, J. Akedo, Int. J. Appl. Ceram. Technol. 3 (2006) 419–427.
[68] S. Baba, J. Akedo, Appl. Surf. Sci. 255 (2009) 9791–9795.
[69] T. Nazarenus, K. Schlesier, S. Biberger, J. Exner, J. Kita, A. Köhler, R. Moos, Int. J. Appl. Ceram. Technol. 19 (2021) 1540–1553.
[70] T. Abe, L. Wu, C. Moriyoshi, Y. Kuroiwa, M. Suzuki, K. Shinoda, R. Aoyagi, J. Akedo, Jpn. J. Appl. Phys. 59 (2020) SPPA04.
[71] X. Wang, R.A.P. Camacho, J.A.S. Oh, Y. Zhang, L. Lu, Funct. Mater. Lett. (2023) 2340003.
[72] D.-M. Chun, S.-H. Ahn, Acta Mater. 59 (2011) 2693–2703.
[73] M. Lebedev, J. Akedo, K. Mori, T. Eiju, J. Vac. Sci. Technol. A: Vacuum, Surfaces, and Films 18 (2000) 563–566.
[74] Y. Furuya, M. Tanaka, S. Kitaoka, M. Hasegawa, Surf. Coating. Technol. (2022) 443.
[75] R. Saunders, S.D. Johnson, D. Schwer, E.A. Patterson, H. Ryou, E.P. Gorzkowski, J. Therm. Spray Technol. 30 (2021) 523–541.
[76] P. Sarobol, M. Chandross, J.D. Carroll, W.M. Mook, D.C. Bufford, B.L. Boyce, K. Hattar, P.G. Kotula, A.C. Hall, J. Therm. Spray Technol. 25 (2016) 82–93.
[77] M. Schubert, M. Hahn, J. Exner, J. Kita, R. Moos, Funct. Mater. Lett. 10 (2017) 1750045.
[78] W.K. Tan, Y. Shigeta, A. Yokoi, G. Kawamura, A. Matsuda, H. Muto, Appl. Surf. Sci. 483 (2019) 212–218.
[79] C. Lee, M.Y. Cho, M. Kim, J. Jang, Y. Oh, K. Oh, S. Kim, B. Park, B. Kim, S.M. Koo, J.M. Oh, D. Lee, Sci. Rep. 9 (2019) 2166.
[80] S.Q. Fan, G.J. Yang, C.J. Li, G.J. Liu, C.X. Li, L.Z. Zhang, J. Therm. Spray Technol. 15 (2006) 513–517.
[81] P. Hartley, G. Parfitt, L. Pollack, Powder Technol. 42 (1985) 35–46.
[82] M. Schubert, J. Kita, C. Münch, R. Moos, Funct. Mater. Lett. 10 (2017) 1750073.
[83] H. Park, J. Heo, F. Cao, J. Kwon, K. Kang, G. Bae, C. Lee, J. Therm. Spray Technol. 22 (2013) 882–891.
[84] M. Suzuki, T. Tsuchiya, J. Akedo, Jpn. J. Appl. Phys. 56 (2017).
[85] J. Lee, C.J. Hogan Jr., Powder Technol. 378 (2021) 400–409.
[86] J. Akedo, M. Lebedev, Jpn. J. Appl. Phys. 41 (2002) 6980–6984.
[87] W.B. Hawley, J. Li, J. Energy Storage 25 (2019) 100862.

[88] T. Jin, Q. Han, L. Jiao, Adv. Mater. 32 (2020) 1806304.
[89] B. Koo, H. Kim, Y. Cho, K.T. Lee, N.S. Choi, J. Cho, Angew. Chem. 124 (2012) 8892–8897.
[90] M.H. Ryou, J. Kim, I. Lee, S. Kim, Y.K. Jeong, S. Hong, J.H. Ryu, T.S. Kim, J.K. Park, H. Lee, Adv. Mater. 25 (2013) 1571–1576.
[91] I. Kim, T.-H. Nam, K.-W. Kim, J.-H. Ahn, D.-S. Park, C. Ahn, B.S. Chun, G. Wang, H.-J. Ahn, Nanoscale Res. Lett. 7 (2012) 1–6.
[92] J.A. Sam Oh, Q. Sun, C. Tian, X. Song, B. Chua, K. Zeng, L. Lu, Mater. Today Energy 27 (2022).
[93] T. Iida, T. Hirono, N. Shibamura, H. Sakaguchi, Electrochemistry 76 (2008) 644–648.
[94] H. Usui, Y. Kashiwa, T. Iida, H. Sakaguchi, J. Power Sources 195 (2010) 3649–3654.
[95] H. Usui, M. Shibata, K. Nakai, H. Sakaguchi, J. Power Sources 196 (2011) 2143–2148.
[96] Y. Iriyama, M. Wadaguchi, K. Yoshida, Y. Yamamoto, M. Motoyama, T. Yamamoto, J. Power Sources 385 (2018) 55–61.
[97] S. Randau, D.A. Weber, O. Kötz, R. Koerver, P. Braun, A. Weber, E. Ivers-Tiffée, T. Adermann, J. Kulisch, W.G. Zeier, F.H. Richter, J. Janek, Nat. Energy 5 (2020) 259–270.
[98] S. Song, H.M. Duong, A.M. Korsunsky, N. Hu, L. Lu, Sci. Rep. 6 (2016) 32330.
[99] X. Lu, C.-L. Tsai, S. Yu, H. He, O. Camara, H. Tempel, Z. Liu, A. Windmüuller, E.V. Alekseev, S. Basak, Funct. Mater. Lett. 15 (2022) 2240001.
[100] X. Lu, C.-L. Tsai, S. Yu, H. He, O. Camara, H. Tempel, Z. Liu, A. Windmüller, E.V. Alekseev, S. Köcher, Funct. Mater. Lett. 15 (2022) 2240002.
[101] Y. Wang, Q. Yi, X. Xu, L. Lu, Funct. Mater. Lett. (2023) 2340002.
[102] D. Hanft, J. Exner, R. Moos, J. Power Sources 361 (2017) 61–69.
[103] L. He, J.A.S. Oh, J.J.J. Chua, H. Zhou, Funct. Mater. Lett. 14 (2020).
[104] L. He, J.A.S. Oh, J.J.J. Chua, H. Zhou, Funct. Mater. Lett. 14 (2020).
[105] S. Basak, V. Migunov, A.H. Tavabi, C. George, Q. Lee, P. Rosi, V. Arszelewska, S. Ganapathy, A. Vijay, F. Ooms, R. Schierholz, H. Tempel, H. Kungl, J. Mayer, R.E. Dunin-Borkowski, R.-A. Eichel, M. Wagemaker, E.M. Kelder, ACS Appl. Energy Mater. 3 (2020) 5101–5106.
[106] N. Kuwata, R. Kumar, K. Toribami, T. Suzuki, T. Hattori, J. Kawamura, Solid State Ionics 177 (2006) 2827–2832.
[107] N. Kuwata, J. Kawamura, K. Toribami, T. Hattori, N. Sata, Electrochem. Commun. 6 (2004) 417–421.
[108] R. Tian, H. Liu, Y. Jiang, J. Chen, X. Tan, G. Liu, L. Zhang, X. Gu, Y. Guo, H. Wang, L. Sun, W. Chu, ACS Appl. Mater. Interfaces 7 (2015) 11377–11386.
[109] H. Kwon, Y. Kim, H. Park, C. Lee, Surf. Coating. Technol. 374 (2019) 493–499.
[110] E. Hüger, C. Jin, H. Schmidt, J. Appl. Electrochem. 52 (2022) 1715–1732.
[111] E.J. Cheng, Y. Kushida, T. Abe, K. Kanamura, ACS Appl. Mater. Interfaces 14 (2022) 40881–40889.
[112] S. Muto, Y. Yamamoto, M. Sakakura, H.-K. Tian, Y. Tateyama, Y. Iriyama, ACS Appl. Energy Mater. (2021).
[113] C.-W. Ahn, J.-J. Choi, J. Ryu, B.-D. Hahn, J.-W. Kim, W.-H. Yoon, J.-H. Choi, D.-S. Park, J. Electrochem. Soc. 162 (2014) A60.
[114] I.S. Erilin, I.N. Burmistrov, D.A. Agarkov, E.A. Agarkova, D.V. Yalovenko, A.A. Solovyev, S.V. Rabotkin, V.E. Pukha, N.V. Lyskov, S.I. Bredikhin, Mater. Lett. 306 (2022).
[115] J. Exner, P. Fuierer, R. Moos, Thin Solid Films 573 (2014) 185–190.
[116] S.H. Cho, Y.J. Yoon, Thin Solid Films 547 (2013) 91–94.
[117] G.-T. Hwang, V. Annapureddy, J.H. Han, D.J. Joe, C. Baek, D.Y. Park, D.H. Kim, J.H. Park, C.K. Jeong, K.-I. Park, J.-J. Choi, D.K. Kim, J. Ryu, K.J. Lee, Adv. Energy Mater. 6 (2016).